

Unravelling quantum carpets: a travelling wave approach

Michael J. W. Hall^{*†}, Martina S. Reineker^{*} and Wolfgang P. Schleich^{*}

^{*}Abteilung für Quantenphysik
Universität Ulm
D-89069 Ulm, Germany

[†]Theoretical Physics, IAS
Australian National University
Canberra ACT 0200, Australia

May 19, 2019

Abstract

Generic channel and ridge structures are known to appear in the time-dependent position probability distribution of a one-dimensional quantum particle confined to a box. These structures are shown to have a detailed quantitative explanation in terms of a travelling-wave decomposition of the probability density, wherein each contributing term corresponds simultaneously to (i) a real wave propagating at a quantised velocity and (ii) to the time-averaged structure of the position distribution along a quantised direction in spacetime. The approach leads to new predictions of channel locations, widths and depths, and is able to provide more structural details than earlier approaches based on partial interference and Wigner functions. Results are also applicable to light diffracted by a periodic grating, and to the quantum rigid rotator.

1 Introduction

The position probability distribution $P(x, t)$ of a one-dimensional quantum particle may be represented as a probability landscape in spacetime, where hills and valleys correspond to regions of high and low probability density respectively. It has recently been discovered that generic two-dimensional structures appear across this probability landscape for a wide variety of potentials and initial conditions [1]-[4]. The highly-patterned nature of these structures has led to them being called “quantum carpets”.

For the simplest case, of a one-dimensional particle moving freely between two end walls, the carpet patterns are linear, with quantised slopes and intercepts [1, 2, 3]. More generally, however, the patterns are curved for particles moving under the influence of a potential [4, 5, 6]. Colour plots of quantum carpets, for a range of examples, may be found in [4] and [5].

Analogous carpet structures also arise for light diffracted by a one-dimensional periodic grating in the paraxial approximation [7, 8]. In this case the time variable t is replaced by the propagation distance z of the diffracted beam, and $P(x, z)$ is the intensity distribution of the beam. Further, it will be seen that a generalised form of these carpet structures arises for the angular distribution $P(\phi, t)$ of the one-dimensional quantum rigid rotator.

Approaches based on interference between energy amplitudes [2, 3], Wigner functions [4], and Greens function degeneracies [5, 9] have been used to explain the observed carpet patterns for various cases, and in particular the observed quantisation of slopes of the linear structures for the confined one-dimensional particle is well understood. However, even in this relatively simple case a number of generic features have not yet been provided with a general explanation, including the depths and widths of channel structures, the decrease of the latter two quantities with slope, and the “chopped” nature of ridge structures (see Fig. 1).

It will be shown in section 2 that such features can be understood to a limited extent by generalising an approach first developed by Berry [2], based on the destructive interference of energy amplitudes (see also [3]). This generalised *destructive interference* approach in particular predicts valley structures along the lines

$$x = kVt + lL, \quad kl = \text{even integer} \quad (1)$$

in spacetime for a particle confined to a one-dimensional box with end walls at

$x = 0$ and $x = L$, providing that the energy amplitude differences $|\psi_n - \psi_{n+k}|$ of the wavefunction are sufficiently small for all n . Here k and l are integers, and

$$V = \pi\hbar/(2ML) \tag{2}$$

is a natural speed defined via the particle mass M .

This destructive interference approach can be further used to show that the average channel depth is expected to decrease as k increases (important in resolving the Olbers-type paradox that any channels at all can be discerned, given that an infinite number of them are predicted by (1) in any given space-time region). Moreover, as shown in the Appendix, it may be generalised to predict the locations of channel and ridge structures for particles moving in *arbitrary* one-dimensional potentials, with results in agreement with [5].

However, the above approach is *not* able to explain a number of other observed features. First, it is completely silent on the location of structures when the condition of small energy amplitude differences is not met. Second, as will be shown by example, it fails to predict *all* observed channel and ridge structures even when this condition *is* met. Finally, the approach yields no information on the shapes and widths of the various structures. A new approach is thus clearly called for.

Such an approach is developed in section 3, based on a representation of the probability landscape as a superposition of travelling waves with velocities which are integer multiples of V , propagating against a constant background. The primary usefulness of this decomposition is that the *average* of the probability distribution along any given direction in spacetime (eg, corresponding to a channel or ridge) is described by at most a *single* one of these travelling waves. In particular, the wave corresponding to velocity kV provides specific, exact information on the average locations, shapes, depths and widths of all channel and ridge structures with slope kV . Connections with the destructive interference approach are briefly discussed.

In section 4 it is shown that each travelling wave can be written as the sum of two Wigner functions plus an energy amplitude term. This form is useful for showing how localisation and symmetry properties of the initial probability distribution can enhance or suppress carpet patterns. In Sec. 5 predictions are verified via the examples of a uniform initial wavefunction and an approximately Gaussian initial wavefunction, for which analytic expressions are obtained for the travelling waves.

Generalisations of the results to periodic gratings and the quantum rigid rotator are given in section 6, with conclusions presented in section 7.

2 Destructive interference approach

2.1 Derivation

Berry derived the locations of channel structures of a one-dimensional particle moving freely between two end walls, for the case of a *uniform* initial wavefunction [2]. Here his derivation is generalised to predict the quantum carpet structure for a broad class of initial wavefunctions, and In the Appendix it is shown how this approach may be further generalised to predict the curved carpet structures corresponding to *arbitrary* one-dimensional potentials.

Schrödinger's equation for a free particle of mass M confined to the interval $(0, L)$, under the usual boundary conditions that the wavefunction vanishes at the endpoints, has the general solution

$$\psi(x, t) = (2/L)^{1/2} \sum_{n=1}^{\infty} \psi_n e^{-i\pi n^2 V t/L} \sin n\pi x/L \quad (3)$$

$$= -i/\sqrt{2L} \left[\sum_{n=1}^{\infty} \psi_n e^{i\phi_+(x,t,n)} - \sum_{n=1}^{\infty} \psi_n e^{i\phi_-(x,t,n)} \right], \quad (4)$$

where ψ_n denotes the n -th energy amplitude, V is the speed defined in (2), and the phases ϕ_{\pm} are given by

$$\phi_{\pm}(x, t, n) = (\pm nx - n^2 V t)\pi/L. \quad (5)$$

The position amplitude $\psi(x, t)$, and hence the position probability distribution $P(x, t) = |\psi(x, t)|^2$, will be small if partial cancellation can be arranged between the two summations in (4). This is possible in particular if the term corresponding to summation index n in the first summation partially cancels with the term corresponding to summation index $n + k$ in the second summation, where k is some fixed integer. Indeed, it is not difficult to show that (4) can be rearranged (to within an overall phase factor) as

$$\psi(x, t) = (2L)^{-1/2} \sum_{n=1}^{\infty} \left[\psi_{n+|k|} e^{i\phi_{\pm}(x,t,n+|k|)} - \psi_n e^{i\phi_{\mp}(x,t,n)} \right]$$

$$+ (2L)^{-1/2} \sum_{n=1}^{|k|} \psi_n e^{i\phi_{\pm}(x,t,n)}, \quad (6)$$

where the upper (lower) phase subscript is chosen when k is positive (negative). Thus significant cancellation between energy amplitudes can take place in the first summation, leading to a small value of $P(x, t)$, providing that the phase-matching condition

$$\phi_+(x, t, n + k) = \phi_-(x, t, n) \quad (\text{mod } 2\pi) \quad (7)$$

is met for all n .

It is the phase condition (7) which leads to (1). In particular, note that channel structures in the probability landscape correspond to spacetime trajectories $x(t)$ along which the position probability density is relatively low, and hence in particular to trajectories for which the phase condition (7) is satisfied at all points. Substituting (5) into (7), differentiating with respect to time, and comparing consecutive values of n , yields the condition $\dot{x}(t) = kV$ for the slope of such a trajectory. Substituting $t = 0$ in (7) further yields, on comparison for consecutive values of n , condition (1).

Note that while condition (1) thus follows from destructive interference between pairs of energy amplitudes in (6), two further conditions are also necessary in general for channel structures to be observed. In particular, substitution of (1) in (6) gives the expression

$$\begin{aligned} \psi(kVt + lL, t) &= (2L)^{-1/2} \sum_{n=1}^{\infty} (-1)^{nl} (\psi_{n+|k|} - \psi_n) e^{-in(n+|k|)\pi Vt/L} \\ &+ (2L)^{-1/2} \sum_{n=1}^{|k|} (-1)^{nl} \psi_n e^{-in(n-|k|)\pi Vt/L} \end{aligned} \quad (8)$$

for the position amplitude along the trajectory. Thus for the trajectory to correspond to a channel one requires further that (i) *the differences* $|\psi_n - \psi_{n+|k|}|$ *are small*, and (ii) *|k| itself is sufficiently small*. These requirements guarantee that the first and second summations in (8) yield, respectively, relatively small contributions to the total amplitude, and hence to $P(x, t)$. They hold for a wide group of initial wavefunctions, as discussed in section 2.2, and hence condition (1) has a wide predictive power.

2.2 Channel depths and ridge heights

Equation (8) leads to a simple estimate of channel depth. In particular, the quadratic n -dependence of the phases in (8) implies that they are quasi-random in time, and hence the average probability density along a given channel can be estimated as

$$\begin{aligned} \overline{P(kVt + lL, t)} &\approx (2L)^{-1} \sum_{n=1}^{\infty} |\psi_n - \psi_{n+|k|}|^2 + (2L)^{-1} \sum_{n=1}^{|k|} |\psi_n|^2 \\ &= L^{-1} \left(1 - \sum_{n=1}^{\infty} \operatorname{Re}\{\psi_n^* \psi_{n+|k|}\} \right). \end{aligned} \quad (9)$$

Note that for slowly varying energy amplitudes this expression will typically increase as $|k|$ increases, i.e., deep channels correspond to small values of $|k|$. It will be seen in section 4 that this expression is close to the exact average depth of the channel.

A particularly simple example is when the initial wavefunction is an equally weighted superposition of N consecutive energy eigenstates, i.e., $\psi_n = 1/\sqrt{N}$ for $M < n \leq M + N$ and $\psi_n = 0$ otherwise, for some $M \geq 0$. From (8) it follows that relatively good destructive interference takes place for $|k| \ll N$, and from (9) that the average density along a channel is approximately given by $|k|/(NL)$. Thus deep channels correspond to small values of $|k|$, as expected. Note moreover from (8) that destructive interference is impossible for $|k| \geq N$, and hence only a finite number of channels can be observed in this case. A previous analytic study of this example for $M = 0$ confirms these results [3].

Constructive interference between energy amplitudes in the first summation in (6) corresponds to adding π to one side of the phase-matching condition (7). It follows that constructive interference takes place along trajectories as per (1), except that the product kl is now restricted to be *odd*. Thus “ridges” are predicted along such lines in the probability landscape, in agreement with numerical observations [1] - [5], [9]. Moreover, the average height of these ridges may be estimated as per for channel depths above, yielding an expression similar to (9) but with subtraction replaced by addition. Thus for the above example the average ridge height is predicted to be $(2N - |k|)/(NL)$ for $|k| \ll N$.

Finally, note that fluctuations of channel depth along a given channel are constrained to be small, simply because they are bounded by the rela-

tively small average probability density (which must remain positive along the channel). In contrast, fluctuations of ridge height are only bounded by the relatively large average ridge height, and indeed are expected to be of the same order from the quasi-random nature of the phases appearing in the analogue of (8) for constructive interference (where the minus sign in the first summation is replaced by a plus sign). It is these relatively large fluctuations which lead to the observed generic “chopped” nature of ridge structures [3].

2.3 Examples

The usefulness and limitations of the generalised destructive interference approach is investigated here via two generic examples. It will be shown in particular that channels are expected as per (1) for well-localised initial wavepackets; and conversely that destructive interference fails to account for all observed channels in the case of wavepackets with periodically spaced energy amplitudes.

Example (i) Momentum amplitudes and localised wavepackets:

The probability landscapes of wavefunctions initially well-localised in a one-dimensional box have been studied in a number of special cases [3, 4, 5, 9]. Here it is shown that the destructive interference approach provides a general explanation of channel locations for *all* initial wavepackets which have a slowly varying momentum amplitude distribution, and for well-localised wavepackets in particular.

Let $\tilde{\psi}(p)$ denote the momentum amplitude distribution of the initial wavepacket, i.e.,

$$\tilde{\psi}(p) = (2\pi\hbar)^{-1/2} \int_{-\infty}^{\infty} e^{-ipx/\hbar} \psi(x, 0) dx. \quad (10)$$

It follows from (3) and (10), recalling that $\psi(x, 0)$ vanishes outside the interval $(0, L)$, that the energy amplitudes ψ_n can be expressed as

$$\psi_n = (2/L)^{1/2} \int_0^L \sin(n\pi x/L) \psi(x, 0) dx \quad (11)$$

$$= i(\pi\hbar/L)^{1/2} [\tilde{\psi}(n\pi\hbar/L) - \tilde{\psi}(-n\pi\hbar/L)]. \quad (12)$$

From (8) and (12) it follows the destructive interference approach predicts channels of slope kV , as per (1), *providing that the momentum amplitude distribution $\tilde{\psi}(p)$ varies sufficiently slowly over any range of length $|k|\pi\hbar/L$.*

In particular, if the initial wavepacket $\psi(x, 0)$ is smooth and well-localised within the box then the momentum amplitude distribution will typically be broad, with root mean square variance Δp say. Thus channels of slope kV are predicted for

$$|k|\pi\hbar/L \ll \Delta p. \quad (13)$$

Noting that the Heisenberg uncertainty relation implies that $\Delta p \geq \hbar/(2\Delta x)$, one in particular expects to see channels of slope kV for all smooth localised wavepackets such that $|k| \ll L/(2\pi\Delta x)$. These general predictions are well borne out by the approximately Gaussian initial wavepackets studied previously [1], [4] - [9].

Example (ii) Periodically spaced energy amplitudes: The second example to be considered here is the case where the non-zero energy amplitudes of the wavefunction are periodically spaced, i.e.,

$$\psi_n = 0 \text{ for } n \neq r \text{ mod } p \quad (14)$$

for some period p and fixed integer r .

The case $p = 1$ is trivial, with channels predicted as per (1) just as before. The case $p = 2$ corresponds to initial wavefunctions which are either symmetric or antisymmetric about $x = L/2$, as r is odd or even respectively, as can be directly seen from the form of the wavefunction in (3). The case $p = 3$ will be seen to be of special significance, providing an example where the destructive interference approach breaks down.

From (14) it is seen that amplitudes ψ_n and $\psi_{n+|k|}$ can only destructively interfere in the first summation in (6) when k is a multiple of the period p and $n = r \text{ mod } p$. Accordingly, substituting pk for k and $pn + r$ for n in the phase-matching condition (7) leads to the modification

$$x = kpVt + lL/p, \quad (k + 2r/p)l = \text{even integer} \quad (15)$$

of (1), for trajectories which correspond to channels in the probability landscape. Condition (15) is equivalent to (1) for $p = 1$. More generally the predicted channel locations depend upon both p and r , have slopes which are multiples of pV , and intersect the x -axis at multiples of L/p .

For example, for $p = 2$ and $r = 1$ (symmetric initial wavefunctions), it follows that channels correspond to the trajectories $x = 2kVt + lL/2$, such that $(k+1)l$ is even. This prediction is equivalent to Eq. (52) of [2], obtained there for the special case of an initially uniform wavefunction.

The case $p = 3$ provides an example which demonstrates a incompleteness of the destructive interference approach. In particular, consider an initial wavefunction given by the equally-weighted superposition

$$\psi(x, 0) = N^{-1/2} \sum_{n=0}^{N-1} \sin[(3n + 1)\pi x/L]. \quad (16)$$

This corresponds to $p = 3$ and $r = 1$ in (14), and hence from (15) *no* channels starting from $x = L/3$ are predicted. However, the density plot of the corresponding probability landscape for this example, shown in Figure 1 for $N = 20$, shows that a channel of slope $-3V$ is in fact associated with this starting point. The appearance of this unexpected channel will be explained in the following section.

3 Travelling wave approach

3.1 Structure function decomposition

It has been seen that the destructive interference approach successfully predicts a number of generic properties of quantum carpets, including the locations of channel and ridge structures and their corresponding average depths and heights. It does not, however, yield information on the shapes and widths of these structures; does not predict *all* observed structures (Figure 1); and is in any case limited in applicability to wavefunctions with energy amplitudes which are slowly varying over ranges of length $|k|$. Thus a new, more general approach is desirable.

To introduce such an approach, it is first convenient to rewrite the wavefunction in (3) in the form [9]

$$\psi(x, t) = -i(2L)^{-1/2} \sum_{n=-\infty}^{\infty} \psi_n e^{i(nx - n^2 Vt)\pi/L}, \quad (17)$$

where one extends the energy amplitude coefficients ψ_n to negative values of n via the definition

$$\psi_{-n} = -\psi_n. \quad (18)$$

From (17) one immediately has

$$P(x, t) = (2L)^{-1} \sum_{m, n=-\infty}^{\infty} \psi_m^* \psi_n e^{-i(m-n)[x - (m+n)Vt]\pi/L} \quad (19)$$

for the position probability distribution. It may be seen that each term in this summation either has no spacetime dependence ($m = n$), or is a plane wave with velocity $(m + n)V$ ($m \neq n$). Collecting the $m = n$ terms into a constant background term, and grouping terms corresponding to waves propagating at velocity kV , one obtains the decomposition

$$P(x, t) = L^{-1} \left[1 + \sum_{k=-\infty}^{\infty} S_k \left(\frac{x - kVt}{L} \right) \right] \quad (20)$$

of the probability landscape, where the “structure functions” S_k are given by

$$S_k(z) = \frac{1}{2} \sum_{m=-\infty}^{\infty} \psi_m^* \psi_{k-m} e^{-i(2m-k)\pi z} - \frac{1}{2} |\psi_{k/2}|^2. \quad (21)$$

Here $\psi_{k/2}$ is defined to be zero when k is odd.

Equation (20) is the travelling wave decomposition referred to in the Introduction. The first term, L^{-1} , is a constant background term for the probability distribution, and the structure function S_k is a real travelling wave travelling at velocity kV . Note that S_k is defined on the entire real axis, and satisfies the relations

$$S_k(z + 1) = (-1)^k S_k(z), \quad S_{-k}(z) = S_k(-z), \quad (22)$$

where the latter of these follows using (18).

The travelling wave decomposition (20) provides a physical picture for the generation of the probability landscape $P(x, t)$, as the superposition of waves of discrete velocities propagating in spacetime against a constant background probability. However, the primary usefulness of this decomposition arises from its relationship to the statistical properties of the probability landscape.

In particular, from (21), the time average of $S_k(z + \alpha t)$ is equal to $S_k(z)$ if $\alpha = 0$ and vanishes otherwise. It follows via (20) that the average of $P(x, t)$ along the linear trajectory $x(t) = x_0 + kVt$ is given by

$$\overline{P(x_0 + kVt, t)} = L^{-1} [1 + S_k(x_0/L)] \quad (23)$$

for any integer k , and by L^{-1} when k is not an integer. Thus the average distribution along any direction in spacetime involves at most *one* structure function.

3.2 Locations, shapes and widths of linear structures

From (23) it is seen that $S_k(z)$ contains all information pertaining to the average properties of linear structures of slope kV in a quantum carpet. In particular, channel/ridge structures are associated with those trajectories $x = x_0 + kVt$ for which x_0/L corresponds to minima/maxima respectively of S_k . Moreover, the average shape of these structures corresponds to the shape of the associated structure function.

For example, $1 + S_{-3}(z)$ is plotted in Figure 2 for the wavefunction (16) (with $N = 20$). The deep maximum in Figure 2 in the vicinity of $z = 1/3$ implies, via relation (23), that a well-defined channel structure of slope $-3V$ crosses the x -axis at $L/3$. This channel is precisely the unexpected channel observed in Figure 1, which was not predicted by the destructive interference approach of section 2. Note also from Figure 2 that a ridge structure immediately parallel to the left of this channel is also predicted, as indeed may also be observed in Figure 1. Since the structure functions in (21) can be trivially evaluated as sums of geometric series for this example, the average properties of all linear structures can in fact be calculated analytically via (23) if desired.

In Figure 3 the travelling wave decomposition (20) is directly illustrated, again for the wavefunction (16) with $N = 20$, where only terms with $|k| \leq 5$ have been included in the summation. Comparison with Figure 1 demonstrates that all linear carpet structures with slope less than or equal to $5V$ in magnitude are reproduced in Figure 3.

Note finally that one can make use of (23) to define the average horizontal width of a given channel or ridge structure. In particular, suppose such a structure corresponds to a trajectory passing through the x -axis at x_0 . Define x_+ and x_- to be the points to the right and left respectively of x_0 for which the average probability distribution first becomes equal to the background probability L^{-1} . The difference $x_+ - x_-$ is then a natural measure of the horizontal width of the structure. From (23) these points correspond to the zeroes of the structure function lying either side of x_0/L , where x_0/L itself corresponds to a minimum or maximum of the structure function. Note for a structure of slope kV that a corresponding measure of width in the direction *perpendicular* to the structure is obtained by dividing the horizontal width by $(1 + k^2V^2)^{1/2}$.

3.3 Connections between the approaches

Since from (23) the structure functions are real, one can rewrite (21) as

$$\begin{aligned} 4S_k(z) + 2|\psi_{k/2}|^2 &= 2 \sum_{m=-\infty}^{\infty} \operatorname{Re} \left\{ \psi_m^* \psi_{k-m} e^{-i(2m-k)\pi z} \right\} \\ &= \sum_{m=-\infty}^{\infty} \left\{ |\psi_{k-m} + \psi_m e^{i(2m-k)\pi z}|^2 - |\psi_{k-m}|^2 - |\psi_m|^2 \right\}. \end{aligned}$$

Replacing m by $m+k$ in the first term of this sum and using (18) then gives an alternate formula for the average probability distribution in (23):

$$\overline{P(x_0 + kVt, t)} = (4L)^{-1} \left[\sum_{m=-\infty}^{\infty} |\psi_m - \psi_{m+k} e^{i(2m+k)\pi x_0/L}|^2 - 2|\psi_{k/2}|^2 \right]. \quad (24)$$

The above expression clearly indicates a link between the average probability distribution and interference of the amplitudes ψ_m and ψ_{m+k} . Further, this interference is seen to be *destructive* when $x_0 = lL$ for some integer l with kl even, thus recovering condition (1) for channel structures. The destructive interference approach is thus a special case of the travelling wave approach, where condition (1) corresponds to particular minima of the structure functions (at $z = l$) for the case of slowly varying energy amplitudes.

Finally, (18) can be used to rewrite (24) in terms of energy amplitudes ψ_m with $m > 0$:

$$\overline{P(kVt + lL, t)} = L^{-1} \operatorname{Re} \left\{ 1 - \sum_{m=1}^{\infty} \psi_m^* \psi_{m+|k|} + \frac{1}{2} \sum_{m=1}^{|k|-1} \sum_{(m \neq |k|/2)} \psi_m^* \psi_{|k|-m} \right\} \quad (25)$$

when kl is an even integer. Thus the approximation in (9) is seen to be quite good for small $|k|$, and indeed is exact for $|k|$ equal to 1 or 2.

4 Properties of structure functions

4.1 Wigner function form

Expression (21) for the structure function S_k is not always convenient to use. It generally involves an infinite summation, and the contributing energy

amplitudes are not always easily calculated. It would therefore be useful to have a formula for S_k which is directly related to the initial wavefunction $\psi(x, 0)$.

To obtain such a formula, first define the normalised wavefunction $\phi(x)$ on the interval $(-L, L)$ by

$$\phi(x) = 2^{-1/2}[\psi(x, 0) - \psi(-x, 0)] \quad (26)$$

$$= L^{-1/2}/(2i) \sum_{n=-\infty}^{\infty} \psi_n e^{in\pi x/L}, \quad (27)$$

where the second line follows via (17) and (18). Thus $\phi(x)$ is an antisymmetric extension of the initial wavefunction $\psi(x, 0)$. Now let $W_\phi(x, p)$ denote the Wigner function of $\phi(x)$ [10]

$$W_\phi(x, p) = (\pi\hbar)^{-1} \int_{-\infty}^{\infty} dy \phi^*(x-y)\phi(x+y)e^{-2ipy/\hbar}. \quad (28)$$

For $0 \leq x < L$ one then has, as shown further below, the remarkable relation

$$S_k(x/L) = \pi\hbar [W_\phi(x, p_k) + (-1)^k W_\phi(x-L, p_k)] - |\psi_{k/2}|^2/2, \quad (29)$$

connecting S_k with W_ϕ , where

$$p_k = \pi\hbar k/(2L) = kMV. \quad (30)$$

This expression can be trivially extended to evaluate $S_k(z)$ for all values of z via the first of the relations in (22).

As will be seen below, (29) provides a very convenient method for evaluating structure functions, and also for analysing the dependence of quantum carpets on various properties of the initial wavefunction. Expansions of the probability distribution $P(x, t)$ in terms of Wigner functions have been previously obtained [4, 11]. However, these expansions lead only to expressions for S_k involving *infinite* sums of Wigner functions, in contrast to (29). The latter may be derived by substituting (26) and (30) into (28) and recalling that $\phi(x)$ vanishes for $|x| \geq L$ by definition, thus yielding

$$\begin{aligned} 4\pi\hbar L W_\phi(x, p_k) &= \sum_{m,n} \psi_m^* \psi_n e^{-i(m-n)\pi x/L} \int_{-M(x)}^{M(x)} dy e^{i(m+n-k)\pi y/L} \\ &= 2 \sum_{m+n \neq k} \psi_m^* \psi_n e^{-i(m-n)\pi x/L} \frac{\sin[(m+n-k)\pi M(x)/L]}{(m+n-k)\pi/L} \\ &\quad + 2 \sum_m \psi_m^* \psi_{k-m} e^{-i(2m-k)\pi x/L} M(x), \end{aligned}$$

where

$$M(x) := \max\{L - |x|, 0\}. \quad (31)$$

Substitution into the righthand side of (29) gives (21) as required.

4.2 Localisation and symmetry effects

To see how localisation and symmetry properties of the initial wavefunction directly affect the structure functions, one may substitute (26) and (28) into (29), to obtain

$$\begin{aligned} S_k(x/L) &= (\pi\hbar/2) \left[W_\psi(x, p_k) + (-1)^k W_\psi(L - x, -p_k) \right] \\ &\quad - (1/2) \left[I_\psi(x, p_k) + |\psi_{k/2}|^2 \right] \end{aligned} \quad (32)$$

for $0 \leq x < L$, where W_ψ denotes the Wigner function of $\psi(x, 0)$, and the “interference” term $I_\psi(x, p_k)$ is given by

$$I_\psi(x, p_k) = \begin{cases} \int_{-\infty}^{\infty} dy \psi^*(y + x, 0) \psi(y - x, 0) e^{i\pi ky/L} + c.c., & 0 \leq x \leq L/2 \\ (-1)^k I(L - x, -p_k), & L/2 < x < L. \end{cases} \quad (33)$$

Now, for example, suppose that the initial wavefunction $\psi(x, 0)$ is well-localised about some point $x_0 \neq L/2$. The corresponding Wigner function $W_\psi(x, p)$ will then be similarly localised, and hence from (23) and (32) one predicts (i) a ridge structure associated with the trajectory $x_0 + kVt$; and (ii) a ridge/channel structure associated with the trajectory $L - x_0 + kVt$ for even/odd values of k . An example verifying this prediction is given in section 5.2 below.

It is also of interest to consider the cases of trajectories of the form $x = lL + kVt$ (arising from the destructive interference approach in section 2). From (22), (32) and (33) one has

$$\begin{aligned} S_k(l) &= (-1)^{kl} S_k(0) \\ &= (-1)^{kl+1} \left[\int_0^L dx P(x, 0) \cos(\pi kx/L) + |\psi_{k/2}|^2/2 \right], \end{aligned} \quad (34)$$

where $P(x, 0)$ is the initial position probability distribution. The average probability density along these trajectories thus only depends on the phase

structure of $\psi(x, 0)$ via $\psi_{k/2}$ (which is zero for odd values of k and typically small in general).

If initial distribution $P(x, 0)$ is well-localised within a region $(x_0 - \delta x, x_0 + \delta x)$ such that

$$\delta x/L \ll |k|^{-1}, \quad (35)$$

then from (34) the average probability density along $x = lL + kVt$ is essentially determined by the properties of the cosine function $\cos \pi kx_0/L$. For example, if x_0 satisfies

$$kx_0/L = j \quad (36)$$

for some integer j , then from (23) and (34) one has

$$\overline{P(lL + kVt, t)} \approx (1 - (-1)^{j+kl})/L, \quad (37)$$

corresponding to channel and ridge structures as $j + kl$ is odd and even respectively (the $\psi_{k/2}$ term has been ignored in (37), as from (11) it is typically negligible for localised wavefunctions). Similarly, if j is replaced by $j + 1/2$ in (36) then the $(-1)^{kl+j}$ term in (37) vanishes, and any linear structure associated with the trajectory is suppressed.

Finally, rather than supposing the initial distribution to be well-localised, consider instead the case where $P(x, 0)$ has an approximate reflection symmetry about some point x^* , i.e.,

$$P(x^* + x, 0) \approx P(x^* - x, 0). \quad (38)$$

Noting that $P(x, 0)$ vanishes outside $(0, L)$ one then has from (34) that

$$\begin{aligned} (-1)^{kl} S_k(l) &\approx - \int_0^\infty dx P(x^* + x, 0) [\cos \pi k(x^* + x)/L \\ &\quad + \cos \pi k(x^* - x)/L] - |\psi_{k/2}|^2/2 \\ &= -2 \cos \frac{\pi kx^*}{L} \int_0^\infty dx P(x^* + x, 0) \cos \frac{\pi kx}{L} - \frac{1}{2} |\psi_{k/2}|^2. \end{aligned} \quad (39)$$

Thus the structure function is modulated by the cosine function $\cos \pi kx^*/L$. Linear structures associated with the trajectories $x = kVt + lL$ are therefore enhanced when $kx^*/L = j$ for some integer j , and suppressed when $kx^*/L = j + 1/2$. Examples of such enhancement/suppression are given in the following section.

5 Examples

5.1 Uniform initial wavefunction

The case $\psi(x, 0) = L^{-1/2}$ on $(0, L)$ was considered by Berry [2], who showed that the corresponding probability landscape was a fractal and explained the observed channel structures via destructive interference (Example (ii) of section 2.3 above). For this case it follows from (11) and (18) that

$$\psi_n = 2\sqrt{2}/(n\pi) \quad (40)$$

for odd n , with ψ_n vanishing for even n . The structure function $S_{2k}(z)$ can be evaluated via any of (21), (29) or (32), to give

$$S_{2k}(z) = 2(\pi k)^{-1} \sin[2\pi k \min\{z, 1 - z\}] - \delta_{k0} - |\psi_k|^2/2 \quad (41)$$

for $0 \leq z < 1$, where δ_{kl} is the Kronecker delta and $\sin[x]/x$ is evaluated as 1 for $x = 0$. As usual this may be extended to other values of z via (22).

In Figure 4 (41) is plotted for $k = 1, 2$ and 3. It is seen that while channels are associated with trajectories $x = 2kVt + lL/2$ for even values of $(k+1)l$, as predicted in Example (ii) of section 2.3, these channels are relatively broad and shallow. Indeed the average probability density along these channels follow from (22), (23) and (41) as just the background probability $1/L$ for even k , and $[1 - 4/(\pi k)^2]/L$ for odd k . Channel visibility thus decreases rapidly as $|k|$ increases.

Since the initial probability distribution is symmetric about $x^* = L/2$ for this example, one expects from (39) that channels with slopes of $(2k+1)V$ are suppressed. Indeed, as is most easily seen from (24) (recalling ψ_n vanishes for even values of n), one finds $S_{2k+1}(z) \equiv 0$. Hence *no* linear structures of slope $(2k+1)V$ are predicted, and (20) and (41) then yield the surprisingly simple decomposition

$$P(x, t) = 2 \sum_{k=-\infty}^{\infty} (\pi k L)^{-1} \sigma(x - kVt) \sin[2\pi k(x - kVt)/L] + [1 - 2\sigma(x)]/L \quad (42)$$

of the fractal probability landscape, where $\sigma(x)$ is defined to be +1, 0, and -1 as the fractional part of x/L is respectively less than, equal to, or greater than 1/2.

5.2 Gaussian initial wavefunctions

Consider now the initial wavefunction

$$\psi(x, 0) = K(2\pi\sigma^2)^{-1/4} e^{-(x-\bar{x})^2/(4\sigma^2)} e^{i\bar{p}x}, \quad (43)$$

where $0 < x < L$ and K is a normalisation constant. It will be assumed that $\sigma \ll \bar{x}, L - \bar{x}$, i.e., that the wavefunction is well-localised on the interval. One may then make the extremely good approximation $K = 1$, so that $\psi(x, 0)$ is effectively a Gaussian wavepacket centred at \bar{x} with average momentum \bar{p} .

It is easiest to evaluate the structure functions for this case via (32) and (33), where one makes the (again extremely good) approximation that (43) can be extended over the entire x -axis. Performing the resulting Gaussian integrals then yields

$$S_k\left(\frac{x}{L}\right) \approx \frac{1}{2} \left[e^{-\frac{(x-\bar{x})^2}{2\sigma^2}} e^{-\frac{2\sigma^2(p_k-\bar{p})^2}{\hbar^2}} + (-1)^k \left[e^{-\frac{(L-x-\bar{x})^2}{2\sigma^2}} e^{-\frac{2\sigma^2(p_k+\bar{p})^2}{\hbar^2}} \right] \right] \\ - \begin{cases} e^{-\frac{x^2}{2\sigma^2}} e^{-\frac{\pi^2 k^2 \sigma^2}{2L^2}} \cos \frac{2}{\hbar} (p_k \bar{x} - \bar{p}x), & 0 \leq x \leq \frac{L}{2} \\ (-1)^k e^{-\frac{(L-x)^2}{2\sigma^2}} e^{-\frac{\pi^2 k^2 \sigma^2}{2L^2}} \cos \frac{2}{\hbar} (p_k \bar{x} + \bar{p}(L-x)), & \frac{L}{2} < x < L. \end{cases} \quad (44)$$

The term $-(1/2)|\psi_{k/2}|^2$ in (32) has been ignored, as it vanishes for odd k and from (10) and (12) is only of order $\sigma/L \ll 1$ for even k .

The structure function $S_1(z)$ is plotted in Figure 5 with $\bar{x} = L/3$ and $\sigma = L/40$, for the cases $\bar{p} = 0$ (dashed line) and $\bar{p} = 15\pi\hbar/L$ (solid line). In the latter case it is seen that there is a deep channel associated with the trajectory $x = Vt$, flanked by a high ridge on the left and a moderate ridge on the right. Further, from (22) one has $S_{-1}(1+z) = S_1(1-z)$, and hence there is, conversely, a high ridge associated with the trajectory $x = L - Vt$, flanked by a deep channel on the right and a moderate channel on the left. These predicted features following from Figure 5 may be directly observed in Figure 6, where the probability landscape corresponding to initial wavefunction (43) is plotted for $\bar{x} = L/3$ and $\bar{p} = 15\pi\hbar/L$. The structure functions thus accurately predict the shapes of the observed linear structures.

For the $\bar{p} = 0$ case (dashed line) in Figure 5 it is seen that as well as channel and ridge structures at the endpoints, there is a ridge associated with the trajectory $x = L/3 + Vt$, and a channel associated with the trajectory $x = 2L/3 + Vt$. These latter structures correspond to the Wigner

functions $W_\psi(x_0, p_k)$ and $W_\psi(L - x_0, p_k)$ discussed in section 4.2 for localised wavefunctions, and can again be observed in a plot of the probability landscape. The corresponding structures for the $\bar{p} = 15\pi\hbar/L$ case are observed to be much less pronounced. This is because $W_\psi(\bar{x}, p)$ is localised about $p = \bar{p}$, and is thus relatively small at $p = p_1$.

Gaussian initial wavefunctions also provide an example of the prediction in (37) for well localised initial wavefunctions. In particular, from (44) (recalling the assumption $\sigma \ll \bar{x}, L - \bar{x}$), one finds that

$$S_k(0) \approx -e^{-\frac{\pi^2 k^2 \sigma^2}{2L^2}} \cos \pi k \bar{x} / L. \quad (45)$$

Hence (37) follows whenever conditions (35) and (36) are satisfied (with $\delta x = \sigma$ and $x_0 = \bar{x}$). Further, channels and ridges associated with trajectories $x = kVt + lL$ are seen to be suppressed if $\pi k \bar{x} / L = j + 1/2$ for some integer j . Since Gaussian initial wavefunctions are not only localised about \bar{x} , but are approximately symmetric about \bar{x} , one may also obtain (45) from (39), with $x^* = \bar{x}$.

6 Periodic gratings and rigid rotators

Consider now a plane wave of wavelength λ incident on a one-dimensional periodic grating, of period $2L$ in the x direction. In the paraxial approximation the amplitude of the diffracted light then has the general form

$$\hat{\phi}(x, z) = (2L)^{-1/2} \sum_{n=-\infty}^{\infty} \hat{\phi}_n e^{i(nx - n^2 Vz)\pi/L}, \quad (46)$$

where z measures distance propagated perpendicularly to the grating, the Fourier coefficients $\hat{\phi}_n$ are determined by the initial diffracted wave $\hat{\phi}(x, 0)$, and $V = \lambda/(4L)$.

Clearly (46) is formally similar to (17) for a quantum particle moving freely between two endwalls, and indeed analogues of quantum carpets in the grating context have been previously observed and investigated [7, 8]. The significant differences between (46) and (17) are (i) $\hat{\phi}(x, z)$ is periodic on the entire x axis whereas $\psi(x, t)$ vanishes outside the interval $(0, L)$; and (ii) the coefficients $\hat{\phi}_n$ need not be antisymmetric as per (18).

Many of the results of sections 3 and 4 may be directly translated into the grating context. For example, the light intensity distribution $I(x, z) = |\hat{\phi}(x, z)|^2$ has the travelling wave decomposition

$$I(x, z) = (2L)^{-1} \left[I_0 + \sum_{k=-\infty}^{\infty} \hat{S}_k \left(\frac{x - kVz}{L} \right) \right] \quad (47)$$

in analogy to (20), where I_0 is the integrated light intensity per period of the grating and \hat{S}_k is given by (21) with ψ_n replaced by $\sqrt{2}\hat{\phi}_n$. Similarly, the analogue of (23) is

$$\overline{I(x_0 + kVz, z)} = (2L)^{-1} [I_0 + \hat{S}_k(x_0/L)], \quad (48)$$

and thus the structure function \hat{S}_k determines the average locations, shapes, etc of relatively dark and bright structures of slope kV in the x - z plane.

However, while one may also write down a result analogous to (29), an *alternative* Wigner function expression for the structure functions is more useful in the grating context. In particular, define the *periodic* Wigner function

$$W_{\hat{\phi}}(x, p) = \pi^{-1} \int_{-L}^L dy \hat{\phi}^*(x - y, 0) \hat{\phi}(x + y, 0) e^{-2ipy}. \quad (49)$$

This differs from (28) in that $\hat{\phi}$ does *not* vanish outside the interval $(-L, L)$. One may then show, similarly to the proof of (29), that

$$\hat{S}_k(x/L) = \pi W_{\hat{\phi}}(x, \pi k/(2L)) - |\hat{\phi}_{k/2}|^2, \quad (50)$$

where $\hat{\phi}_{k/2}$ is defined to vanish for odd k .

As an example of (50), suppose that a plane wave is incident on a sinusoidal phase grating, as studied in [8], i.e.,

$$\hat{\phi}(x, 0) = (I_0/2L)^{1/2} e^{i\alpha \cos(\pi x/L)}. \quad (51)$$

Substitution into (49) and using the standard Bessel integral

$$\int_0^\pi d\theta \cos[k\theta - a \sin \theta] = \pi J_k(a) \quad (52)$$

then yields, via (48) and (50),

$$\overline{I(x_0 + kVz, z)} = I_0/(2L) \left[1 + (-1)^k J_k(2\alpha \sin[\pi x_0/L]) - |\hat{\phi}_{k/2}|^2 \right]. \quad (53)$$

Here $|\hat{\phi}_{k/2}|$ is zero for odd k , and equal to $J_{k/2}(\alpha)$ for even k [8].

The last term of (53) provides a correction to equation (25) of [8], where the average intensity along the trajectory $x = x_0 + kVz$ was calculated for the same example. More generally, (50) provides a convenient way to calculate the structure function directly from the initial amplitude $\hat{\phi}(x, 0)$, and (47) provides a simple decomposition of the intensity distribution as a sum of travelling waves.

The above results may be immediately translated into the context of the two-dimensional quantum rigid rotator, with Hamiltonian $H = J_z^2/(2I)$. In particular, $\hat{\phi}(\theta, t)$ may be interpreted as the time-dependent phase amplitude of the rotator, where one takes $L = \pi$ and $V = \hbar^2/(2I)$. The carpet structures for this case lie on the cylinder generated by the phase and time coordinates θ and t .

7 Conclusions

The carpet structure of a quantum particle confined between two endwalls has been greatly elucidated by the travelling wave decomposition (20) of the probability density, and the details afforded by this decomposition are seen to go well beyond the ambit of the destructive interference approach. In particular, the structure functions S_k in (20) provide *all* information pertaining to the average properties of linear structures in the probability landscape.

The structure functions may be evaluated either from the energy amplitudes of the wavefunction, via (21); or from the initial wavefunction, via (32). The latter formula permits the dependence of generic features of carpet patterns to be directly determined from corresponding properties of $\psi(x, 0)$. Similarly, for the periodic grating and quantum rigid rotator one may use (50) to directly evaluate structure functions from $\hat{\phi}(x, 0)$.

One advantage remaining to the destructive interference approach is that it may be generalised to predict the carpet structure of semiclassical wavepackets moving in arbitrary one-dimensional potentials (see Appendix). It is hoped that a corresponding generalisation of the travelling wave decomposition (20) can be found.

Acknowledgements

We are grateful to Professor Berry for a copy of [8] prior to publication. MH acknowledges the support of the Alexander von Humboldt Foundation.

Appendix

It will be briefly indicated here how the destructive interference approach of section 2 may be generalised to predict the *curved* carpet structures arising in the probability landscapes of one-dimensional particles moving in general potentials [4, 5, 6]. For semi-classical wavepackets the analysis is very similar to that of subsection 2.1, and the results agree with those of Kaplan et al [5] obtained by consideration of degeneracies of the propagator for $P(x, t)$.

Now, for high energies the n -th energy eigenstate of a particle moving in a one-dimensional potential $U(x)$ with two classical turning points is well approximated as [12]

$$\psi_n(x) = 2[M/T_n p_n(x)]^{1/2} \sin[\hbar^{-1} \int_{x_n}^x p(x) dx + \pi/4], \quad (54)$$

where M is the particle mass; T_n , $p_n(x)$ and x_n are the period, momentum and leftmost turning point respectively of a corresponding classical orbit of energy E_n ; and E_n is implicitly defined by the Bohr-Sommerfeld rule

$$\oint p_n(x) dx = (n + 1/2)2\pi\hbar. \quad (55)$$

The appearance of the sine function in (54) is analogous to that in (3), and for an initial superposition $\psi(x, 0) = \sum c_n \psi_n(x)$ of such states one can easily obtain the analog of (6):

$$\begin{aligned} \psi(x, t) &= \sum_{n=1}^{\infty} \left[A_{n+|k|}(x) e^{i\phi_{\pm}(x, t, n+|k|)} - A_n(x) e^{i\phi_{\mp}(x, t, n)} \right] \\ &+ \sum_{n=1}^{|k|} A_n(x) e^{i\phi_{\pm}(x, t, n)}, \end{aligned} \quad (56)$$

where

$$A_n(x) = [M/T_n p_n(x)]^{1/2} c_n, \quad (57)$$

$$\phi_{\pm}(x, t, n) = \pm \hbar^{-1} \int_{x_n}^x p_n(x) dx - \hbar^{-1} E_n t \pm \pi/4. \quad (58)$$

As in (6), the upper (lower) phase subscript is chosen in (56) when k is positive (negative), and an overall phase factor has been dropped.

Destructive interference in the first summation in (56), giving rise to a channel structure, can take place along a spacetime trajectory $x_k(t)$ if the

phase condition (7) holds for $\phi_{\pm}(x, t, n)$ defined in (58) (providing that the amplitude functions $A_n(x)$ in (57) vary sufficiently slowly with n). Substituting (58) into (7) and differentiating with respect to t yields the condition

$$\frac{dx_k(t)}{dt} = \pm \frac{E_{n+|k|} - E_n}{p_{n+|k|}(x_k) + p_n(x_k)} \quad (59)$$

for the trajectory $x_k(t)$, where the $+/-$ sign is chosen according to whether k is positive/negative. Moreover, if the trajectory passes through point x_0 at time t_0 , one requires from (7) and (58) that

$$\left[(E_{n+k} - E_n)t_0 - \int_{x_n}^{x_0} p_n(x)dx - \int_{x_{n+k}}^{x_0} p_{n+k}(x)dx \right] / \hbar = \pi/2 \bmod 2\pi. \quad (60)$$

For the case of a potential energy which is symmetric about x_0 , this expression may be simplified via (55) to give

$$(E_{n+k} - E_n)t_0/\hbar = (n + k/2 + 1)\pi \bmod 2\pi. \quad (61)$$

Channel structures for various potentials have been numerically observed for a number of examples [4, 5, 6], and (59) has been previously derived in [5], via a decomposition of the probability distribution rather than of $\psi(x, t)$ (which produces an extra set of trajectories, discarded as “classical”). Here it is seen that (59) arises directly from destructive interference of energy amplitudes, in a manner entirely analogous to the case of the particle in a one-dimensional box.

It is hoped to further investigate conditions (59) and (60) elsewhere. Here a simple prediction generated by (59) will be pointed out. In particular, if the energy eigenvalues E_n increase slowly over ranges of length $|k|$ (at least for values of n for which the amplitudes $A_n(x)$ are significant), and $p_n(x)$ varies slowly over such ranges, then from (59) one has $dx_k/dt \approx k(dE_n/dn)/(2p_n(x_k))$. Thus, if two channels corresponding to two values k and k' intersect at some point in spacetime, their slopes at the point of intersection are predicted to be approximately in the ratio

$$(dx_k/dt)/(dx_{k'}/dt) \approx k/k'. \quad (62)$$

This provides a simple test of the applicability of this approach to a given quantum carpet structure: the strongest channels, corresponding to small

values of $|k|$, are predicted to intersect with slopes related by simple rational numbers. Note from (56) that conditions (59) and (60) for destructive interference need in fact only hold over the range of n for which the amplitudes $A_n(x)$ are significant, to ensure effective destructive interference. This is fortunate, as these conditions cannot in general hold for all n ; however, it implies that this approach can in general only be applicable to superpositions of a relatively narrow band of energy eigenstates.

References

- [1] Kinzel W 1995 *Phys. Bl.* **51** 1190 [in German]
- [2] Berry M V 1996 *J. Phys. A* **29** 6617-6629
- [3] Grossmann F, Rost J-M and Schleich W P 1997 *J. Phys. A* **30** L277-L283
- [4] Stifter P, Leichtle C, Schleich W P and Marklof J 1997 *Z. Naturf.* **52a** 377-385 [in German]
- [5] Kaplan A E, Stifter P, van Leeuwen K A H, Lamb Jr. W E and Schleich W P 1998 *Phys. Scr.* **T76** 93-97
- [6] Loinaz W and Newman T J 1999 quant-ph/9902039
- [7] Berry M V and Klein S 1996 *J. Mod. Opt.* **43** 2139-2164
- [8] Berry M V and Bodenschatz E 1999 *J. Mod. Opt.* **46** 349-365
- [9] Marzoli I, Bialynicki-Birula I, Friesch O M, Kaplan A E and Schleich W P 1998 quant-ph/9804015
- [10] Hillery M, O'Connell R F, Scully M O and Wigner E P 1984 *Phys. Rep.* **106** 121-167
- [11] Marzoli I, Saif F, Bialynicki-Birula I, Friesch O M, Kaplan A E and Schleich W P 1998 *Acta Phys. Slov.* **48** 1-11
- [12] Davydov A S 1976 *Quantum Mechanics, 2nd edn* (Oxford: Pergamon Press) section III.23

FIGURE CAPTIONS

Figure 1. Density plot of (part of) the probability landscape for the initial wavefunction in (16), with $N = 20$. The dark channel observed to run from the bottom righthand corner to the top lefthand corner of the plot corresponds to the trajectory $x = L/3 - 3Vt$, and is not predicted by the destructive interference approach.

Figure 2. Plot of $1+S_{-3}(z)$ for the initial wavefunction in (16), with $N = 20$. From (23), the sharp minimum in the vicinity of $z = 1/3$ corresponds to a channel in the probability landscape, along the trajectory $x = L/3 - 3Vt$ (as observed in Figure 1).

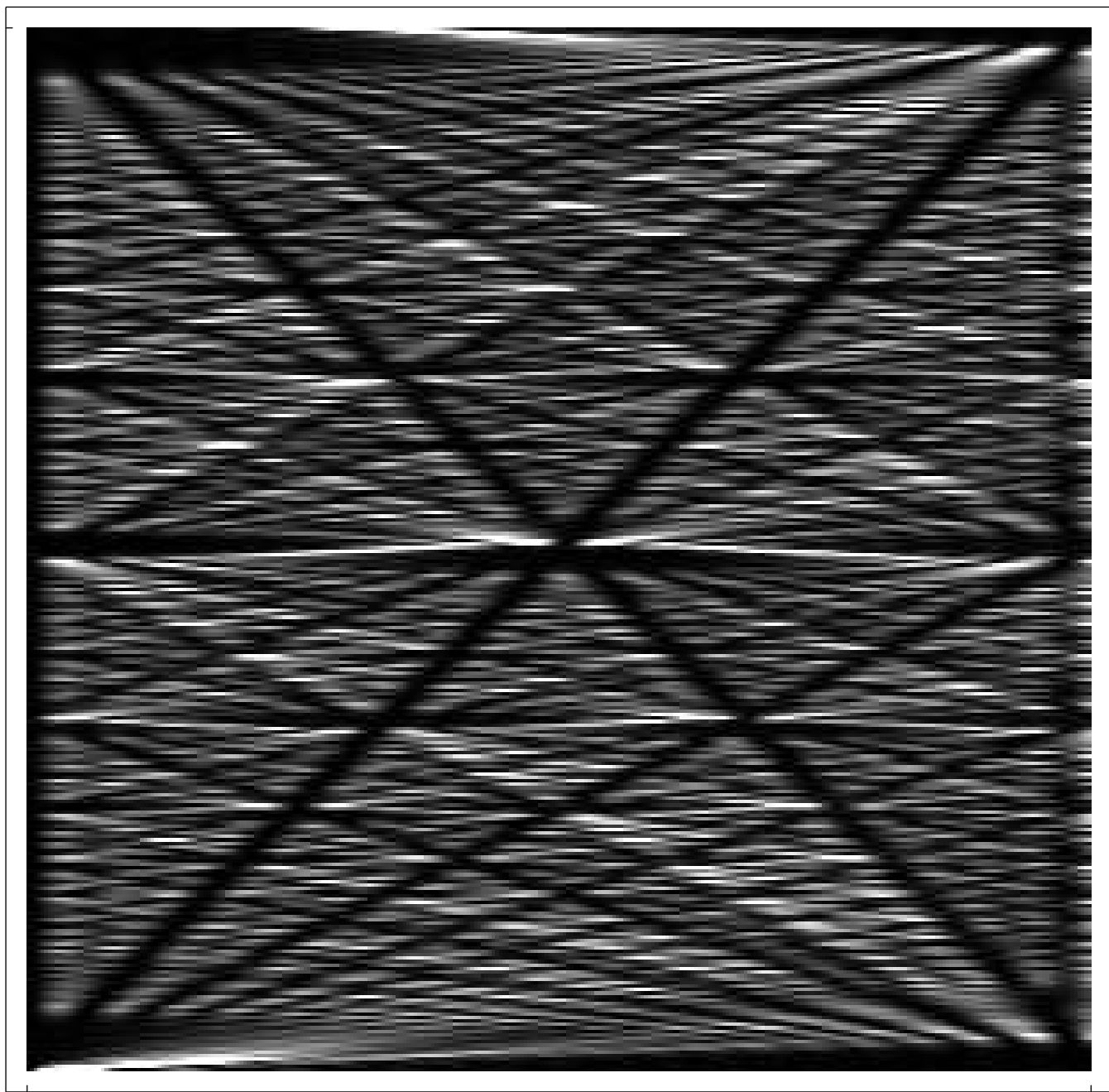
Figure 3. Approximate reconstruction of the density plot in Figure 1 via the travelling wave decomposition (20), where only terms with $|k| \leq 5$ have been included. All linear structures of slope less than or equal to $5V$ in magnitude are successfully reproduced.

Figure 4. The structure functions $S_2(z)$ (solid line), $S_4(z)$ (dot-dashed line) and $S_6(z)$ (dotted line) for the case of a uniform initial wavefunction, plotted via (41).

Figure 5. The structure function $S_1(z)$ for the approximate Gaussian initial wavefunction in (43) with $\bar{x} = L/3$ and $\sigma = L/40$, for the cases $\bar{p} = 0$ (dashed line) and $\bar{p} = 15\pi\hbar/L$ (solid line).

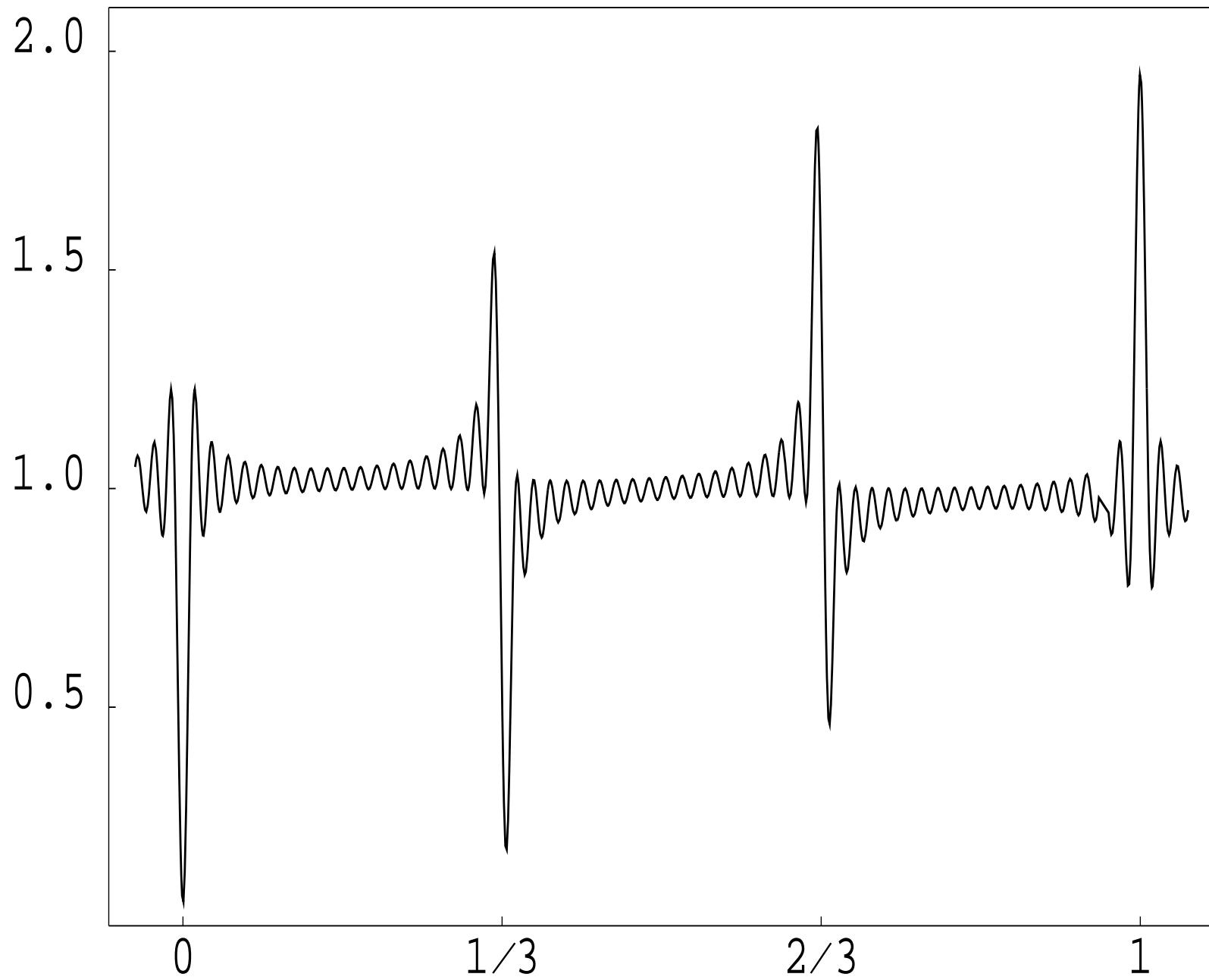
Figure 6. Density plot of the probability landscape for the approximate Gaussian initial wavefunction in (43) with $\bar{x} = L/3$, $\sigma = L/40$ and $\bar{p} = 15\pi\hbar/L$. The detailed shape of the linear structure running from the bottom lefthand corner to the top righthand corner corresponds to that of the structure function of Figure 5 (solid line) in the neighbourhood of $z = 0$.

L/9V

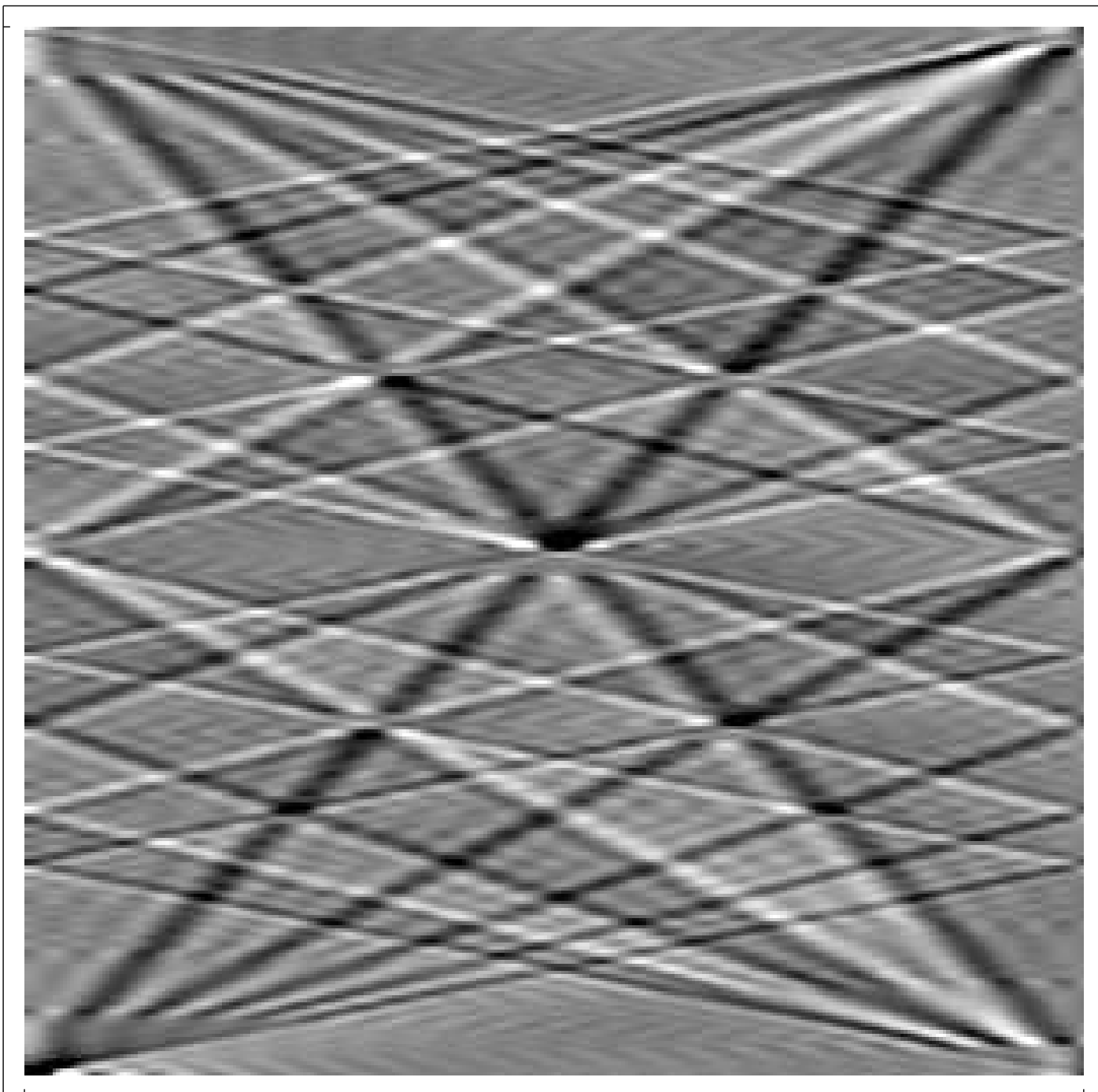


0

L/3

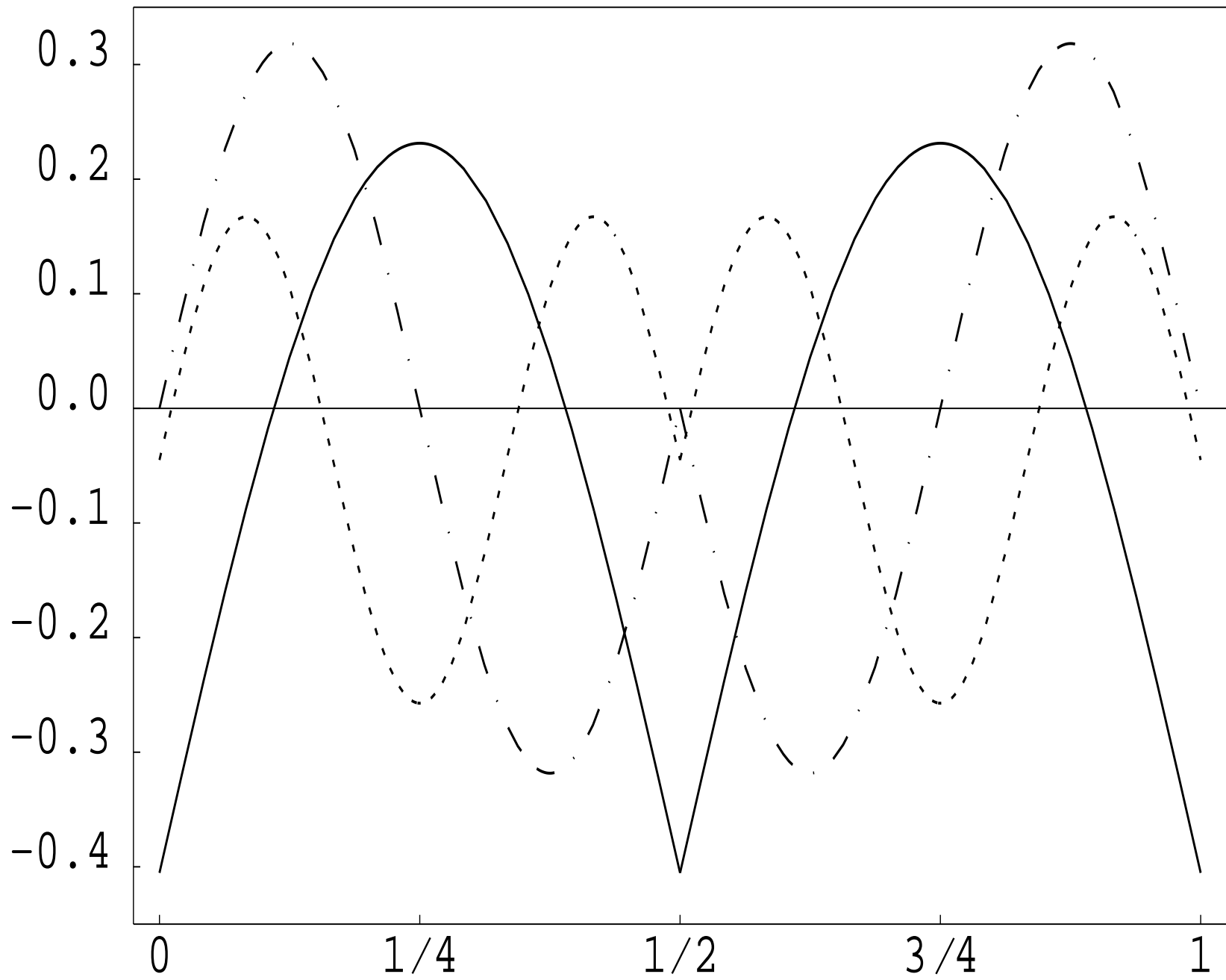


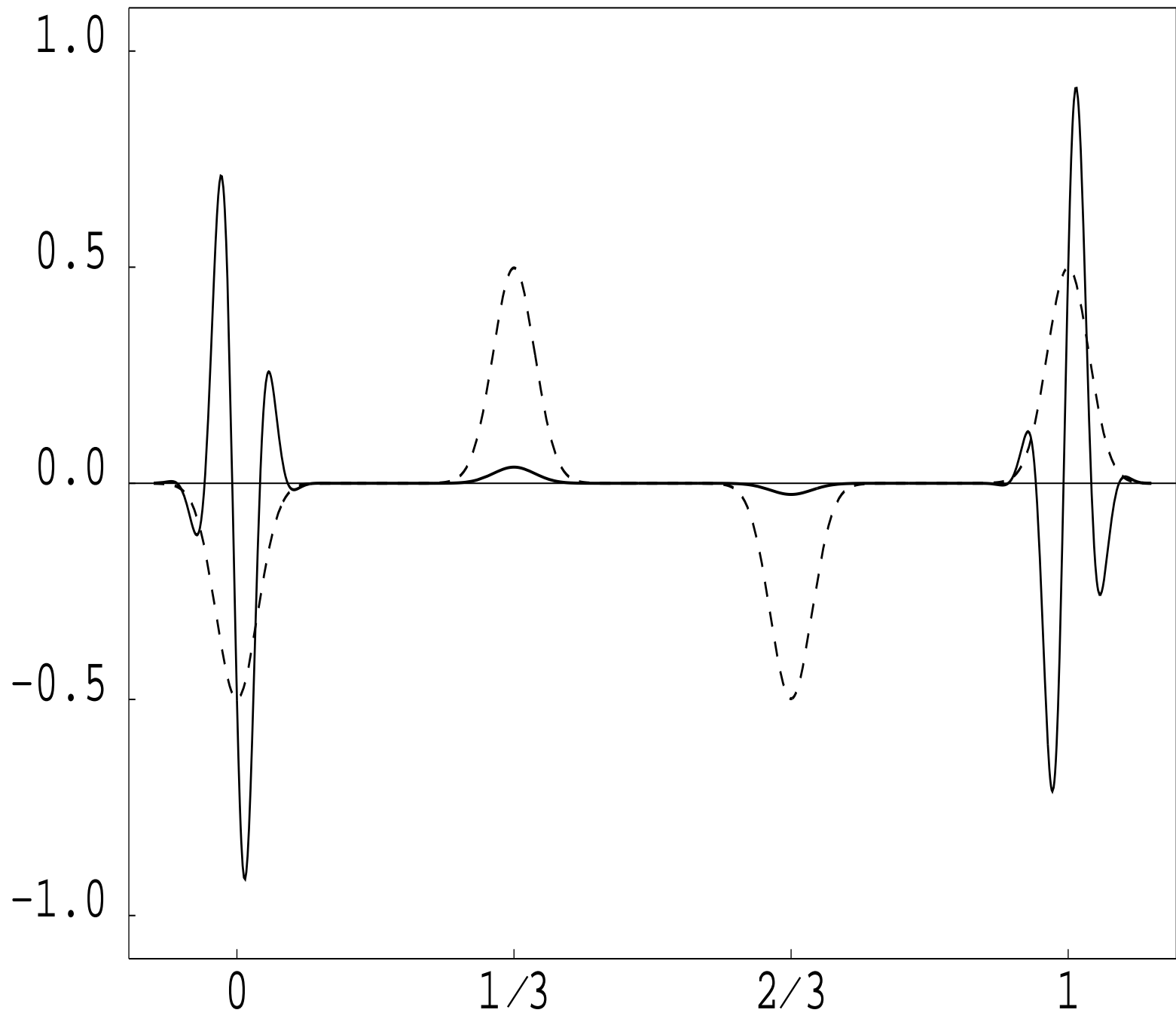
L/9V



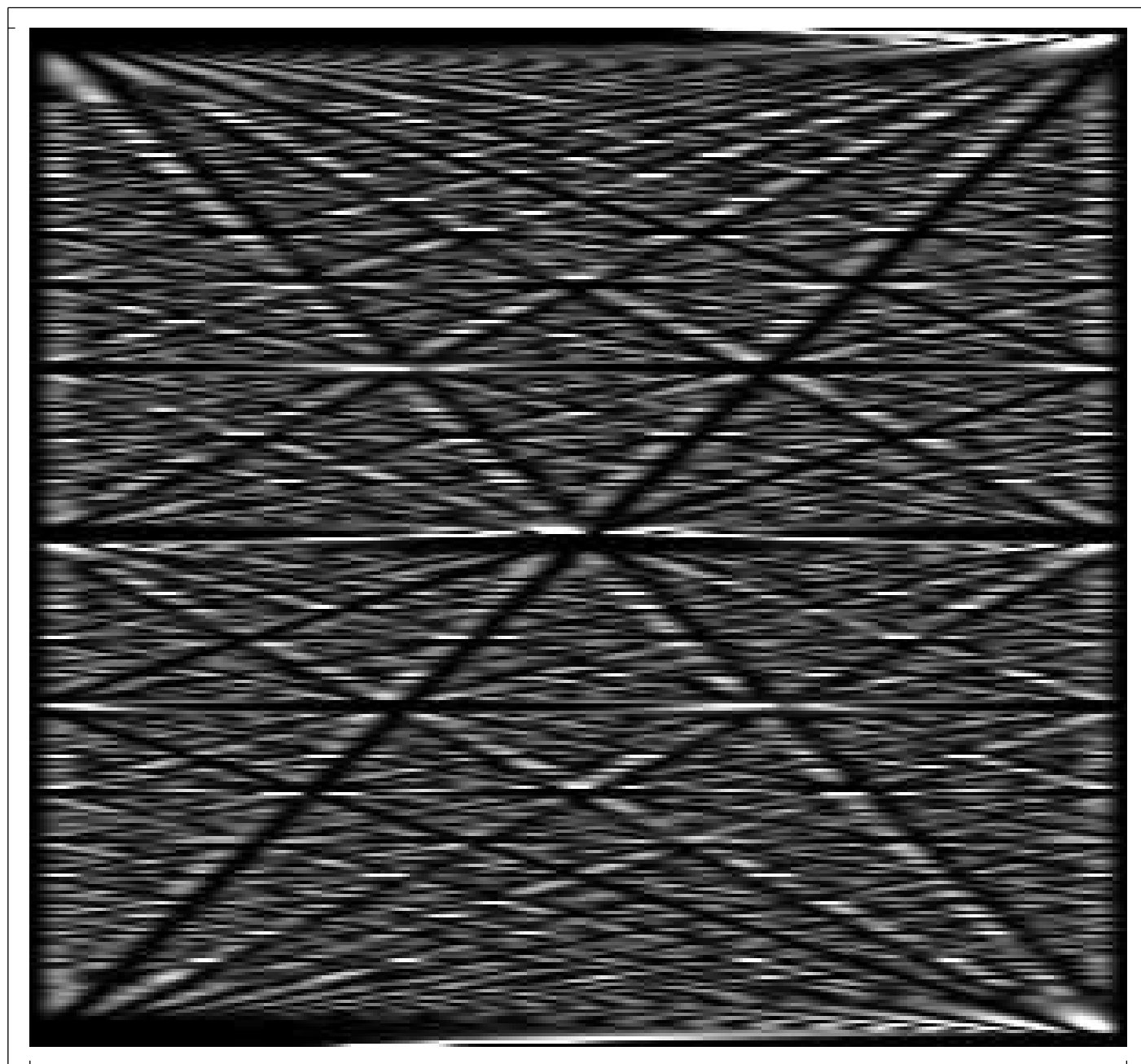
0

L/3





L/V



0

L